CHAPTER IV

RESULTS AND DISCUSSION

4.1 Synthesis of 25,27 – [*N*,*N*′-di-((2-ethoxy)benzyl)propylenediamine] -26,28-dimethoxy-*p*-*tert*-butylcalix[4]arene dihydrochloride (7, L.2HCl)

2-((2′-bromo)ethoxy)benzaldehyde (1) was prepared by previously described procedures [67]. When **1** reacted with *p*-*tert*-butylcalix[4]arene in the presence of K_2CO_3 as base in CH_3CN, 1,3-dialdehyde calix[4]arene **3** was obtained in 50%. The two -OH groups at the lower rim of **3** was then modified to $-OCH_3$ by methylating with CH_3I in the presence of BaO and *t*-BuOK. The 1,3-dimethylated dialdehyde derivative **5** was obtained in 28%. From ^{1}H NMR spectrum of **5** in Figure A.3, there are three broad signals due to *tert*-butyl protons at 0.86, 1.04 and 1.27 ppm. This suggests that calix[4]arene is not in a cone conformation. In addition, signals in non-aromatic regions are broad. The $-OCH_3$ signal appears as a broad peak at 3.82 ppm. These features indicate that the *p*-*tert*-butylcalix[4]arene moiety are moving within the NMR time scale due to the lack of hydrogen bonding interactions among each arene unit. The elemental analysis result, however, agrees with the proposed structure.

Preparation of Schiff base compound **6** was carried out by dropwise addition of the methanolic solution of 1,3-diaminopropane into the CH_3CN solution of 1,3-dimethylated dialdehyde **5** and heating at reflux for 2 days. The compound **6** was obtained in 55%. The ^{1}H NMR spectrum of **6** is shown in Figure A.4. The characteristic singlet peak of HC=N appears at 8.65 ppm. The broad singlets due to ROAr-*t*-C_4H_9 and CH_3OAr-*t*-C_4H_9 appear at 0.79 to 1.32 ppm. The complication of the spectrum may stem from simultaneous existence of more than one conformation of the calix[4]arene unit which occurred *via* arene ring rotation. The elemental analysis result of the compound **6** agrees well with the proposed structure.

The Schiff base **6** was then reduced with $NaBH_4$ in CH_2Cl_2 under nitrogen atmosphere for 2 hours and protonated with 2% HCl in CH_3OH. The ammonium

derivative, 7, was crystallized out of the solution in 77%. MALDI-TOF MS result shows a strong peak due to $[7]^+$ at m/z 1014.2. The ^{1}H NMR spectrum of 7 in $CDCl_3$, DMSO-d_6 and CD_3OD are shown in Figures 4.1, 4.2 and 4.3, respectively. The ^{1}H NMR spectrum in aprotic solvent such as $CDCl_3$ shows complicated lines of *t*-butyl signals indicative of coalescence between conformations that stems from the rotation of the phenoxy methyl units due to the absence of intramolecular hydrogen bonding. However, disappearance of the singlet signal due to *H*C=N at 8.65 ppm and appearance of the broad singlet at 10.01 ppm due to the ammonium protons can be observed. The ^{13}C NMR spectrum of 7 depicted in Figure 4.4 shows the signal due to CH_3OAr-*t*-C_4H_9 at 63 ppm. Nevertheless, the CH_3OAr-*t*-C_4H_9 signal in ^{1}H NMR is broad due to the coalescence between "in side" and "out side" conformation [**68**]. In more polar solvent such as DMSO-d_6, and CD_3OD, the ^{1}H NMR spectra of 7 seems to be more resolved and simplified. In the former solvent, there are two broad singlets at 0.98 and 1.27 ppm due to CH_3OAr-*t*-C_4H_9 and ROAr-*t*-C_4H_9, respectively. The signals in the aromatic region are quite broad leading to ambiguity in conformational assignment of the calix[4]arene framework. However, two H-N^+-N signals apperaring at 9.12 and 9.80 ppm are indicative of mixed conformations. Interestingly, the ^{1}H NMR spectrum of 7 in CD_3OD shows two sharp singlets at 0.99 and 1.34 ppm and also two singlets at 7.21 and 6.71 ppm due to ROAr*H* and CH_3OAr*H*, respectively. This is an indication of a cone conformation of the calix[4]arene unit. This evidence suggests the effect of solvent polarity and hydrogen bonding towards the conformational isomerism of the calix[4]arene moiety. It can be useful to compare our results with studies of conformational isomerism in tetramethoxy-*p*-*tert*-butylcalix [4]arene (**8**). The structure of compounds 7 and **8** are shown in Figure 4.5.

The compound **8** has been demonstrated by Reinhoudt et al.[**69**] to have 31 possible conformations in the gas phase. However, the crystal structure of **8** showed that **8** possessed a partial cone conformation in solid state [**70**]. Gutsche [**68**], however, found by ^{1}H NMR experiments that the partial cone conformation was also preferred in $CDCl_3$ solution. Later, Shinkai and his coworkers [**71**] detected by ^{1}H-NMR that the isomer of **8** depended on the polarity of solvents. It was found that the concentration of the "cone" isomer is increased upon increasing solvent polarity.

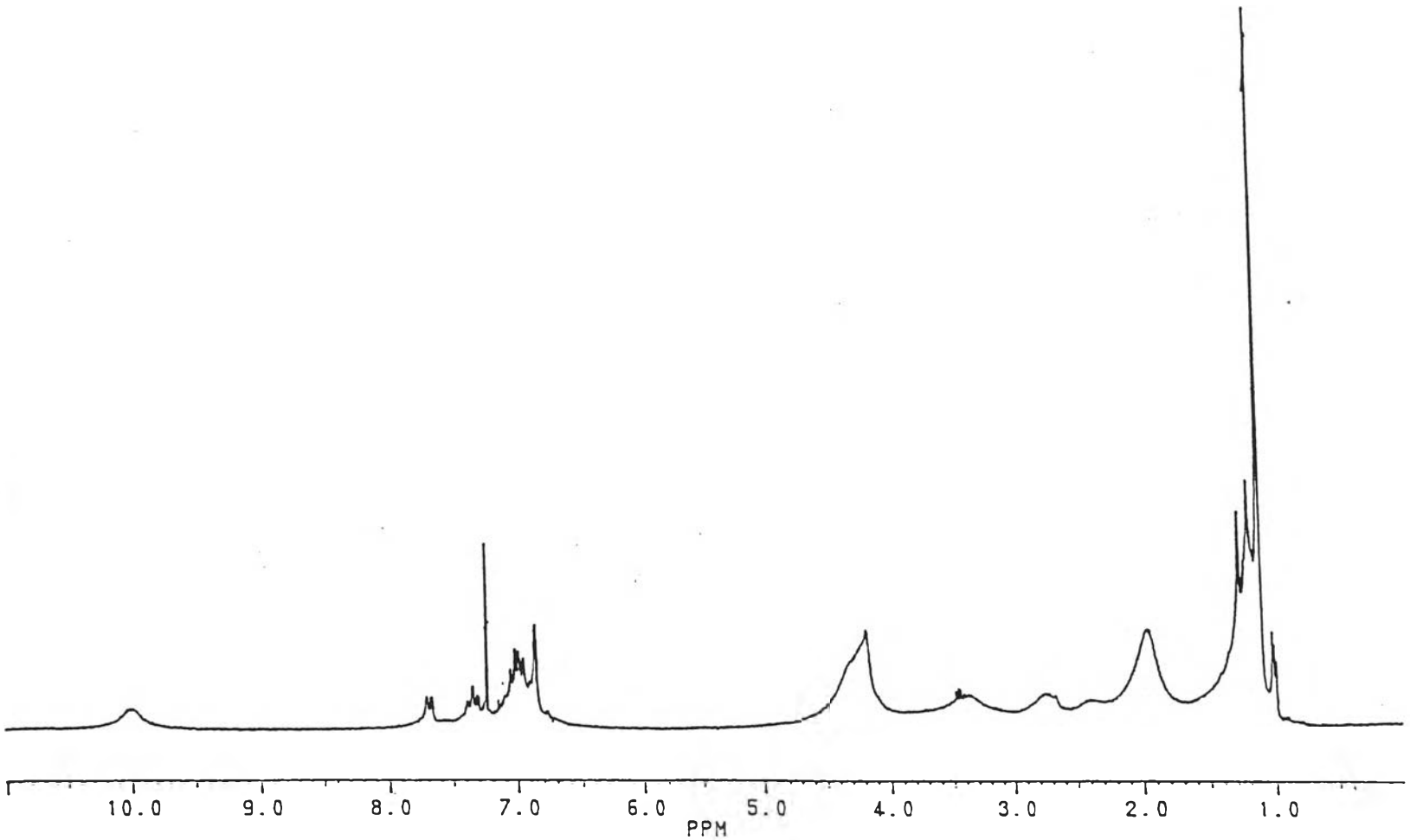

Figure 4.1 ^{1}H NMR spectrum of 7 in $CDCl_3$.

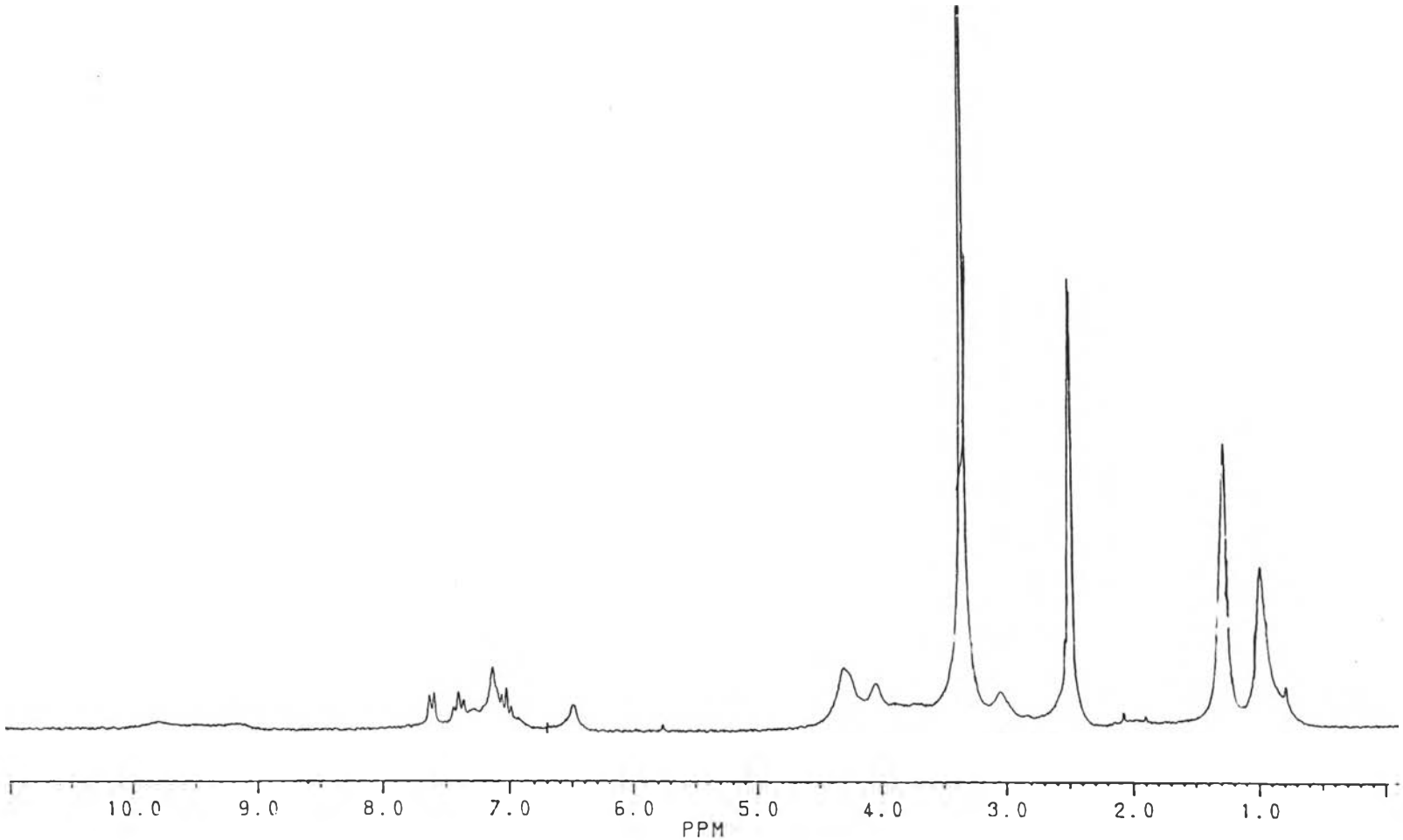

Figure 4.2 ^{1}H NMR spectrum of **7** in DMSO-d_6.

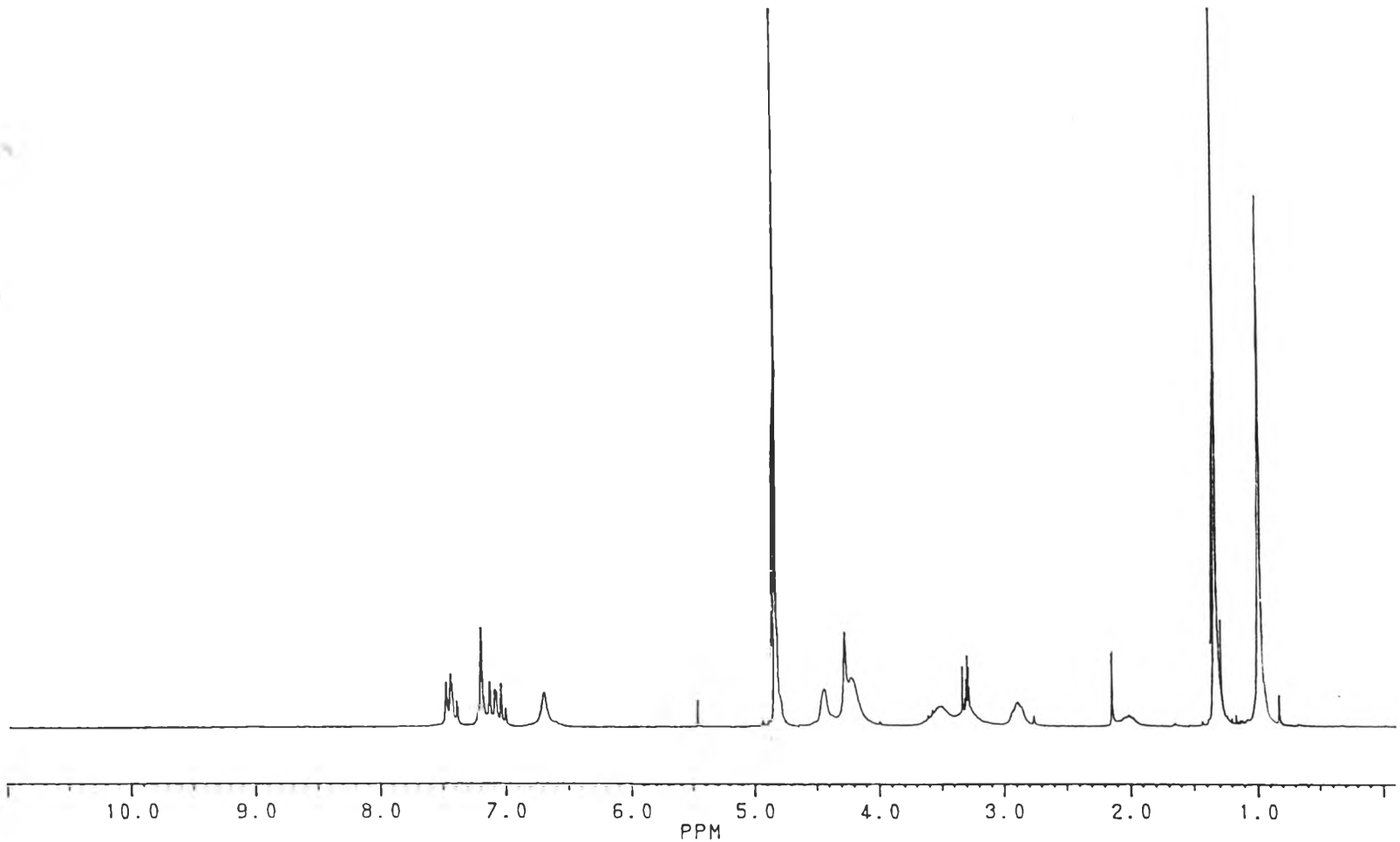

Figure 4.3 ^{1}H NMR spectrum of 7 in CD_3OD.

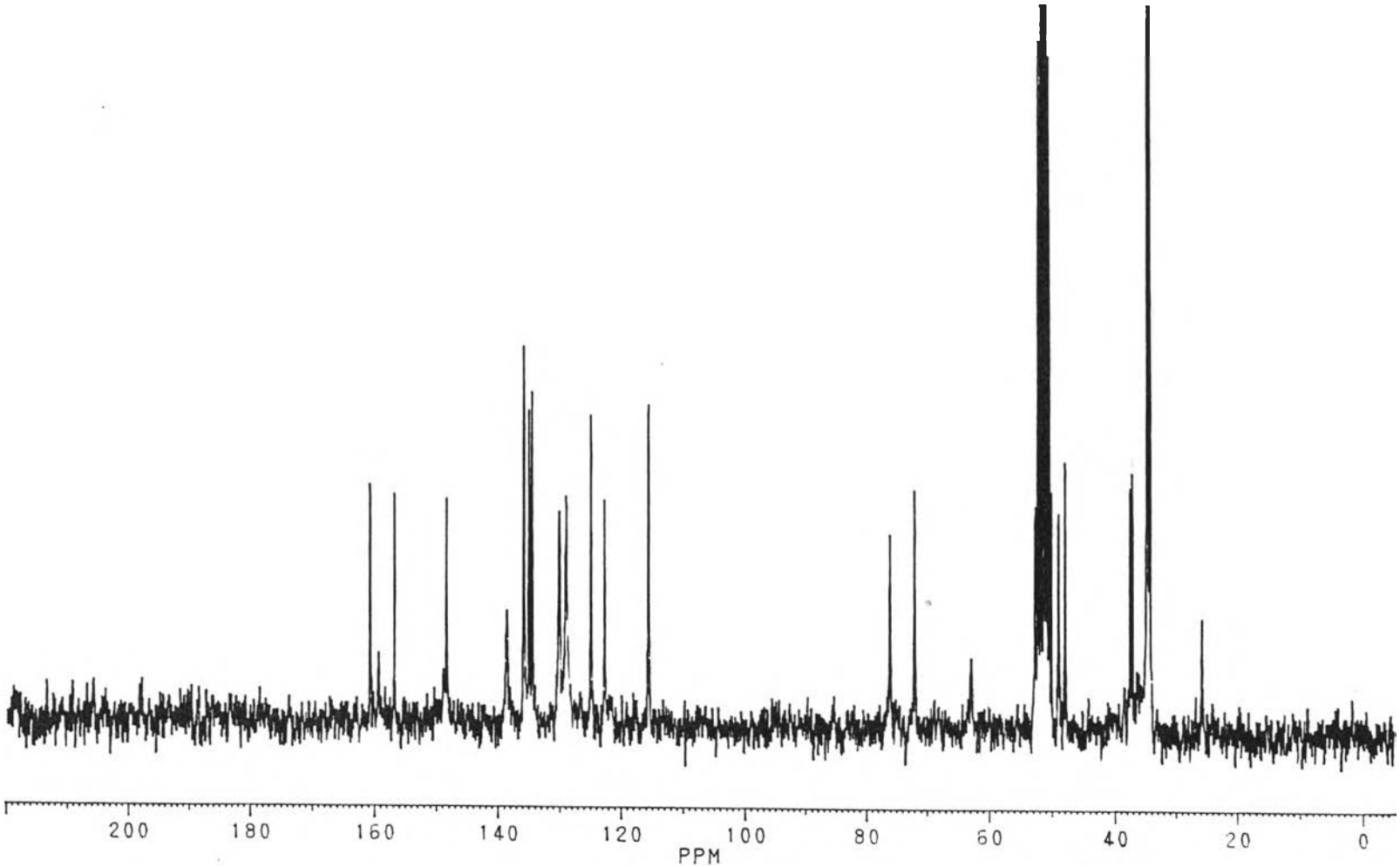

Figure 4.4 ^{13}C NMR spectrum of 7 in CD_3OD.

and thus, formed a polar molecule while a partial cone had one dipole pointed reversed (Figure 4.6) and became a less polar molecule.

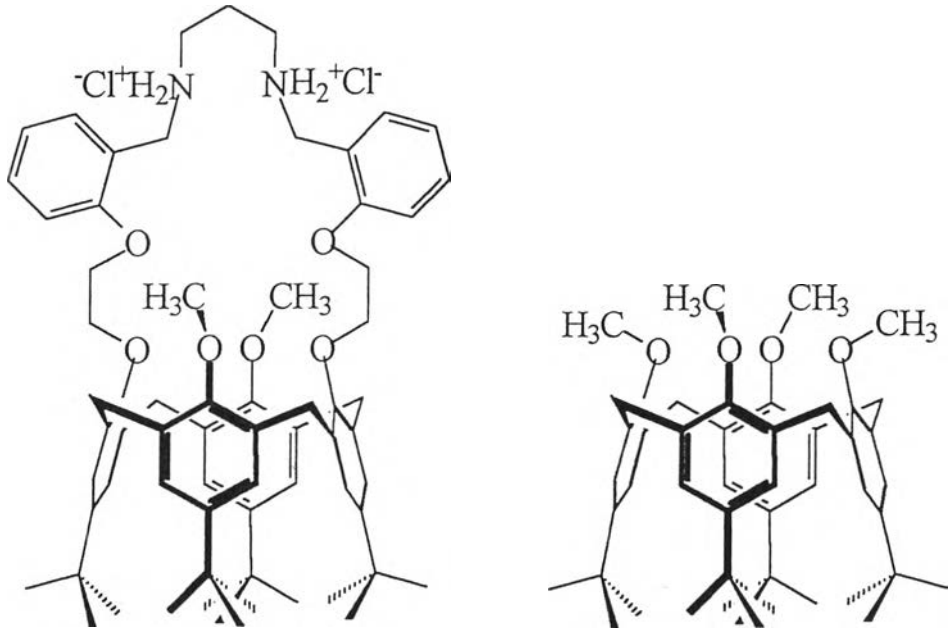

(7) (8)

Figure 4.5 The structure of 25,27-[*N*,*N'*-di-((2-ethoxy)benzyl)propylenediamine]-26,28-dimethoxy-*p-tert*-butylcalix[4]arene dihydrochloride (**7**) and 25,26,27,28-tetramethoxy-*p-tert*-butylcalix[4]arene (**8**).

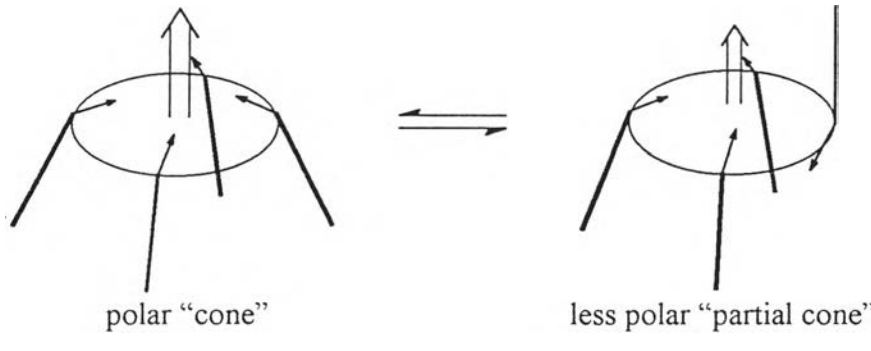

Figure 4.6 Dipole orientation of cone and partial cone conformation.

In our case, ^{1}H NMR spectra of 7 in both polar protic solvent, CD_3OD, and polar aprotic solvent, DMSO-d_6, show different behaviors from those of compound **8** investigated by Shinkai et al [71]. In DMSO-d_6 which is a more polar solvent, the calix[4]arene unit of 7 orientates in mixed conformations while in a less polar solvent, CD_3OD, the calix[4]arene moiety is in a cone conformation. These results give an evidence that besides solvent polarity, intermolecular hydrogen bonding may play an important role in the conformational isomerism of 7. This matter can be further investigated by performing a series of ^{1}H NMR experiments, vide infra.

4.2 ^{1}H NMR studies of the compound 7

4.2.1 Variable ^{1}H NMR experiments for compound 7 in $CDCl_3$

Conformational isomerism of 7 in $CDCl_3$ was studied by variable temperature ^{1}H NMR experiments. The spectra were recorded at 27, 0, -15, -25, -35 and –40 °C as illustrated in Figure 4.7. Changes in every region of the spectra can be observed significantly. The signals due to CH_3OAr-*t*-C_4H_9 and ROAr-*t*-C_4H_9 became more resolved, but they were somewhat broad and split into four distinct lines at –40 °C. The signals in the methylene region and the aromatic region were complicated when the temperature was lowered. The splitting of *H*-N$^+$-*H* protons into 2 broad peaks at 9.91 and 10.18 ppm can also be noted at temperature below –15 °C. These results support the conformational coalescence of calix[4]arene compartment in the compound 7 in $CDCl_3$. Unfortunately, the broad characters of the signals prohibited us to estimate the contribution of each conformation.

4.2.2 Addition of CD_3OD and DMSO-d_6 in the $CDCl_3$ solution of 7

From the spectrum of 7 in CD_3OD, we believe that hydrogen bonding must involve in the sharpness of the signals. Addition of CD_3OD in the $CDCl_3$ solution of 7 may give some clues about intermolecular hydrogen bonding interactions. When CD_3OD was added gradually (5, 10, 15, 20, 25, 30, 40 and 100 μL, respectively), features of ^{1}H NMR spectra of 7 have changed tremendously as shown in Figure 4.8.

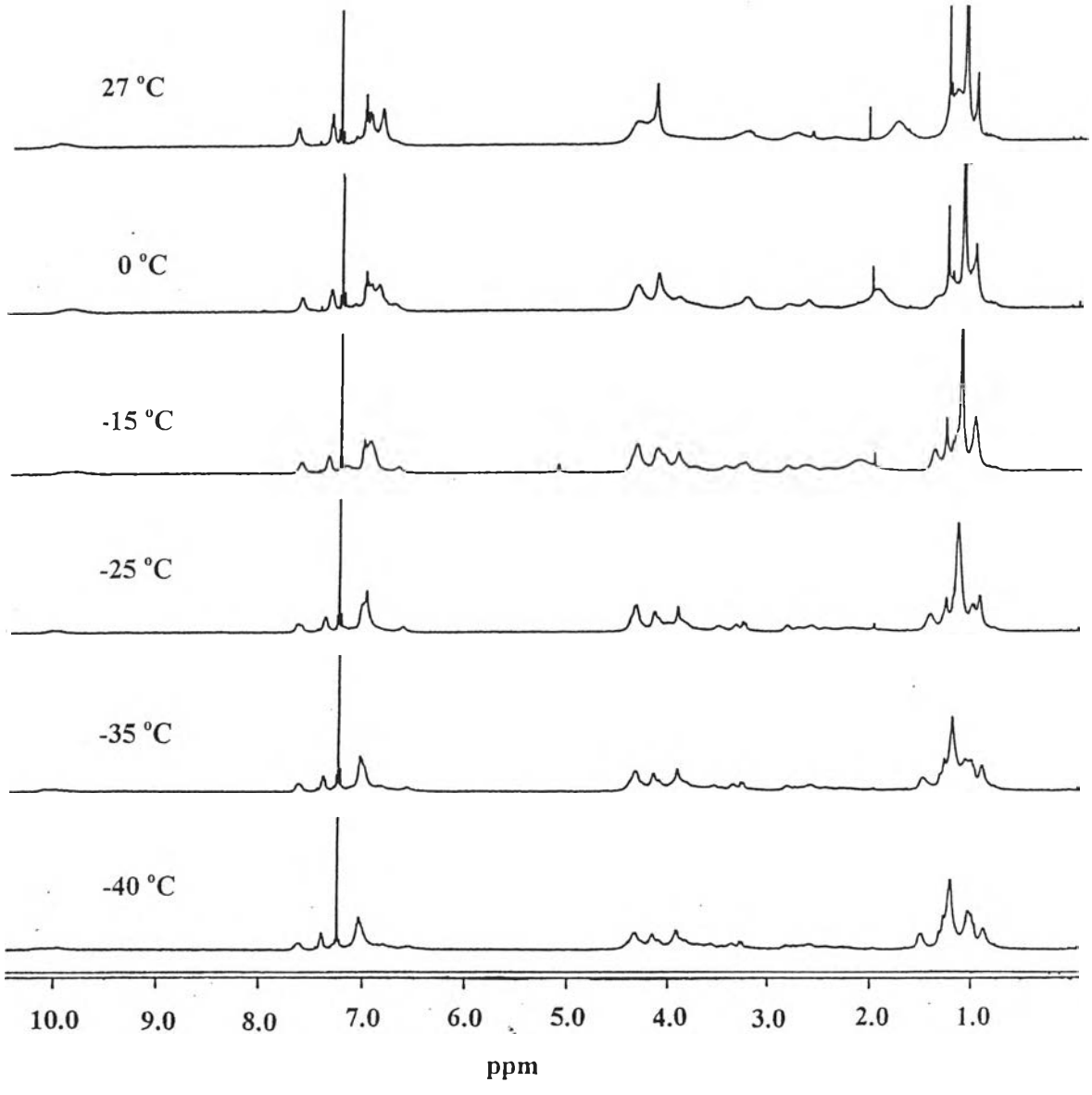

Figure 4.7 ^{1}H NMR spectra of compound 7 in $CDCl_3$ at various temperatures.

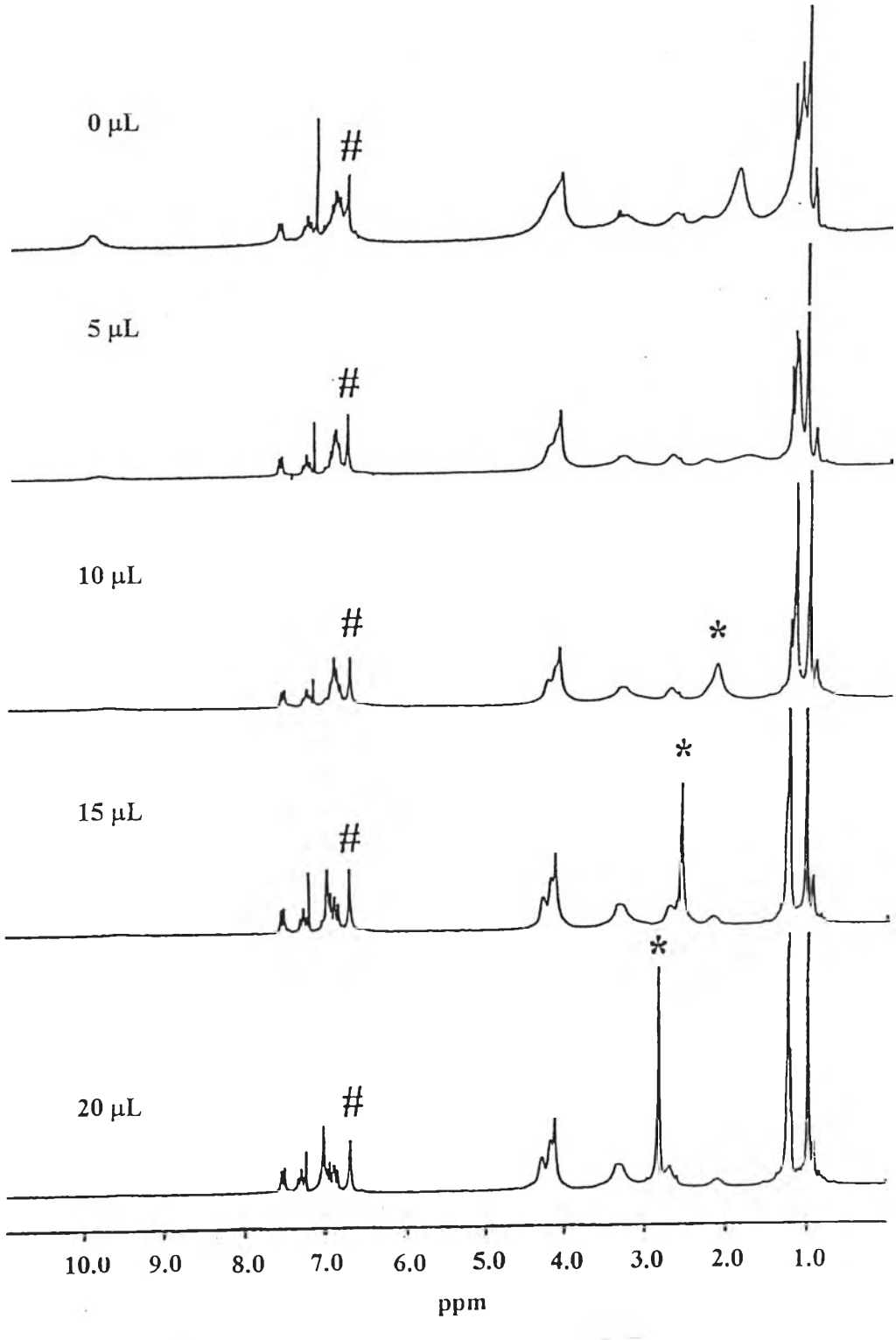

Figure 4.8 ^{1}H NMR spectra of compound **7** in $CDCl_3$ when various amount of CD_3OD was added (Parts of CH_3OAr-*t*-C_4H_9 and $ROAr$-*t*-C_4H_9 were cut off.).

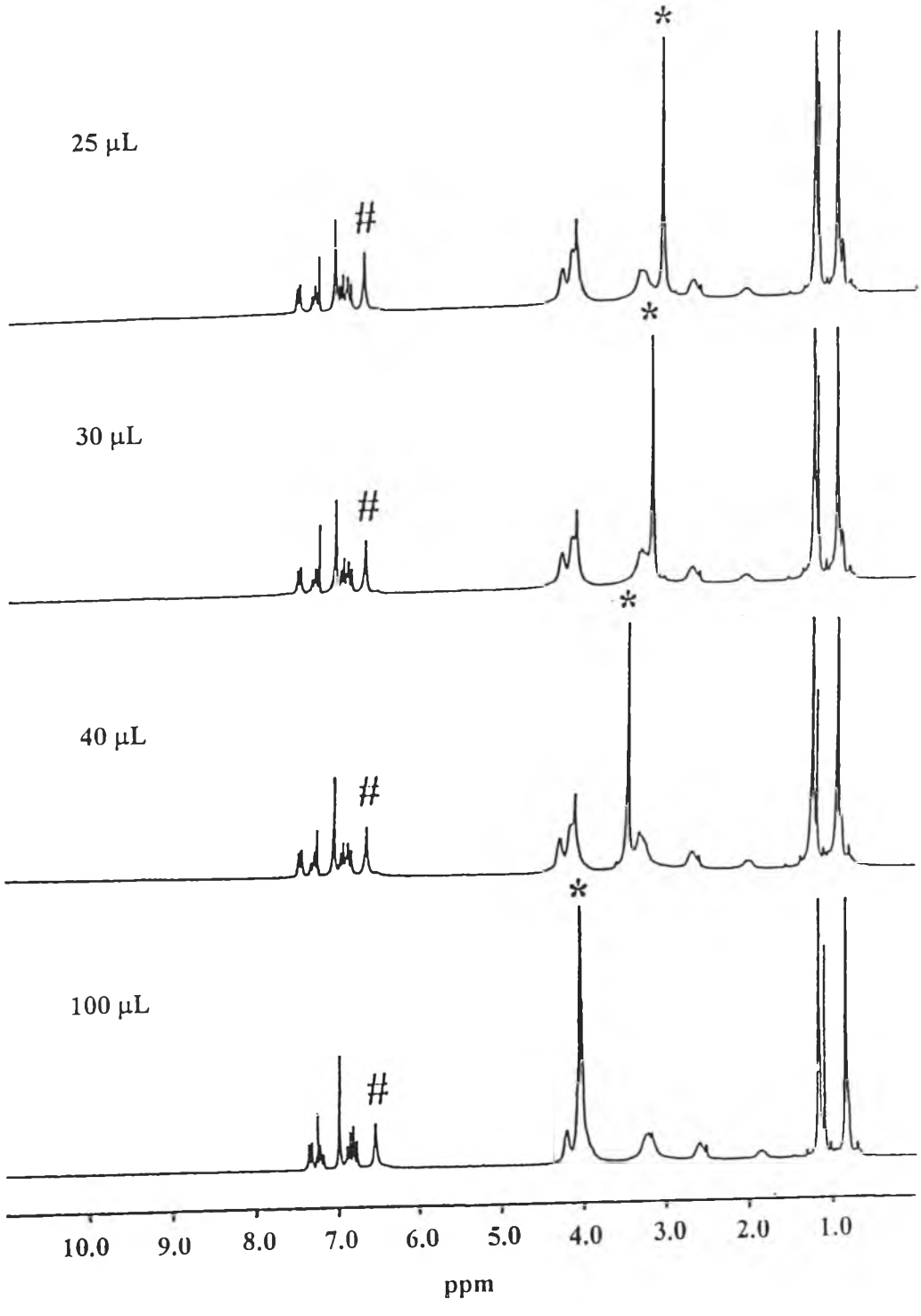

Figure 4.8 (continued).

The signals due to CH_3OAr-*t*-C_4H_9 and ROAr-*t*-C_4H_9 were resolved and appeared as two singlet peaks. In order to differentiate the peak positions for ROAr*H*, CH_3OAr*H*, ROAr-*t*-C_4H_9 and CH_3OAr-*t*-C_4H_9 (singlet) sigals, controlled experiments were carried out with 25,27-[*N,N'*-di-(2-ethoxybenzyl)propylenediamine]-*p-tert*-butylcalix[4]arene dihydrochloride (**9**) [**60**]. Compound **9** possessed intramolecular hydrogen bonding between phenoxy oxygen and phenoxy protons. The results in Figure A.8 show that there is no movement of the singlet peaks in both aromatic and methyl regions and suggest that addition of CD_3OD does not affect the intramolecular hydrogen bonding. For compound 7 in Figure 4.8, the singlet at ≈ 0.9 ppm and the singlet at ≈ 6.7 ppm shifted dramatically upon increasing the amount of CD_3OD. These two signals which were perturbed by addition of CD_3OD should belong to CH_3OAr-*t*-C_4H_9 and CH_3OAr*H*, respectively. The ROAr-*t*-C_4H_9 and the ROAr*H* signals should not move significantly due to the bulkiness the phenyl rings which was attached by a long alkyl chain. In addition gradual addition of CH_3OH into the $CDCl_3$ solution of 7 does nnot result in shifting of the methyl signal and signifies that CH_3OH does not include into the calix[4]arene cavity.

The first thing that could occur when CD_3OD was added was the exchange of protons between CD_3OD and $R_2N^+H_2$ to generate CD_3OH. The CD_3O*H* signal (labeled *) can be observed when > 5 μL of CD_3OD was added. The signal dramatically shifted downfield. Changes of the chemical shifts of CD_3O*H*, ROAr*H*, CH_3OAr*H*, ROAr-*t*-C_4H_9 and CH_3OAr-*t*-C_4H_9 signals of compound 7 are listed in Table 4.1. Intermolecular hydrogen bonding can be recognized by the fact that the shifts due to CD_3O*H* protons depended strongly on CD_3OD concentration [**72**]. Concurrent with the appearance of CD_3O*H*, signals due to *t*-butyl protons became more resolved and appeared as two singlets (a characteristic feature for cone conformation). However, the two signals showed different behavior. The CH_3OAr-*t*-C_4H_9 signal shifted dramatically upfield while ROAr-*t*-C_4H_9 signal moved insignificantly. Concurrently, the signal due to CH_3OAr*H* also shifted largely upfield while the signal due to ROAr*H* shifted insignificantly. This behavior indicated the

Table 4.1 Changes of the chemical shifts of CD_3OH, ROAr*H*, CH_3OArH, ROAr-*t*-C_4H_9 and CH_3OAr-*t*-C_4H_9 signals of the compound 7 in the mixture of $CDCl_3$ and CD_3OD solution.

added CD_3OD (μL)	$\Delta\delta_H$ of CD_3OH (ppm)	$\Delta\delta_H$ of ROAr*H* (ppm)	$\Delta\delta_H$ of CH_3OArH (ppm)	$\Delta\delta_H$ of ROAr-*t*-C_4H_9 (ppm)	$\Delta\delta_H$ of CH_3OAr-*t*-C_4H_9 (ppm)
0	-	*a*	0.00	*b*	*c*
5	*a*	*a*	-0.03	*b*	*c*
10	0.00	0.00	-0.07	0.00	0.00
15	0.41	0.03	-0.12	0.01	-0.04
20	0.69	0.04	-0.15	0.02	-0.06
25	0.90	0.05	-0.17	0.02	-0.08
30	1.02	0.05	-0.19	0.02	-0.09
40	1.30	0.05	-0.22	0.01	-0.12
100	1.90	-0.01	-0.32	-0.06	-0.21

[a] the observed signal is not resolved
[b] the observed signal aggregates with CH_3OAr-*t*-C_4H_9
[c] the observed signal aggregates with ROAr-*t*-C_4H_9.
\+ indicates downfield shift
\- indicates upfield shift

intermolecular hydrogen bonding between CD_3OH and O atoms in CH_3OAr-*t*-C_4H_9 moieties of 7 which prohibited the movement or rotation of the phenoxymethyl rings and held the structure of the calix[4]arene unit in a cone conformation. The hydrogen bonding pattern of 7 and CD_3OH can be proposed as shown in Figure 4.9.

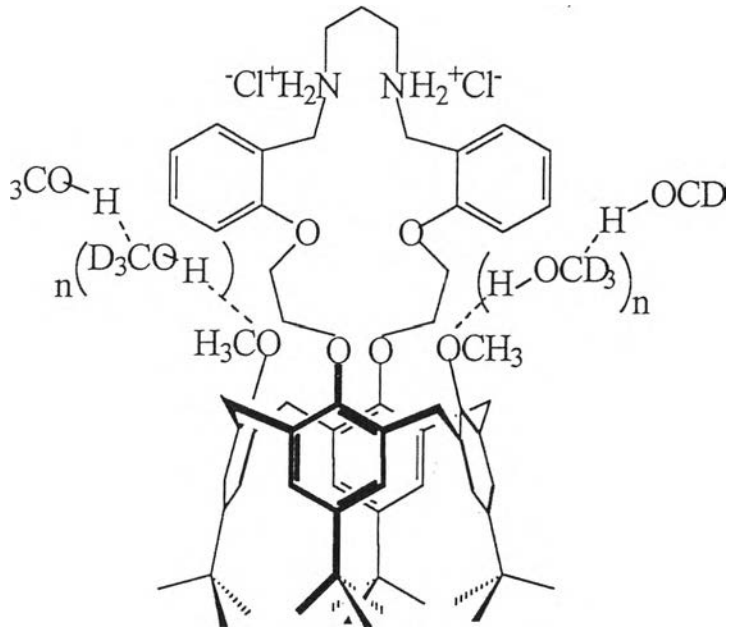

Figure 4.9 The proposed structure of intermolecular hydrogen bonding between compound 7 and CD_3OH.

Addition of DMSO-d_6 in the $CDCl_3$ solution of 7 was performed in a similar manner to the CD_3OD case and the spectra are shown in Figure A.6. Changes in chemical shifts of the spectra are collected in Table 4.2. The signals due to CH_3OAr-*t*-C_4H_9 and ROAr-*t*-C_4H_9 become two broad singlets after addition of 20 μL of DMSO-d_6. The latter shifts more significantly than the former does (Table 4.2). This is opposite to the results obtained when adding CD_3OD. There are also changes in the aromatic region. We can observe a resolved signal of CH_3OArH which is shifted upfield. However, the signal due to ROAr*H* cannot be assigned due to broad characters of aromatic region. The broad nature of these spectra may stem from the lack of intermolecular hydrogen bonding to inhibit the phenoxy ring rotation. After

Table 4.2 Changes of the chemical shifts of N*H*, CH_3OAr*H*, -NCH_2C*H*$_2CH_2$N-ROAr-*t*-C_4*H*$_9$ and CH_3OAr-*t*-C_4*H*$_9$ signals of the compound 7 in the mixture of $CDCl_3$ and DMSO-d_6 solution.

added DMSO-d_6 (μL)	$\Delta\delta_H$ of N*H* (ppm)	$\Delta\delta_H$ of CH_3OAr*H* (ppm)	$\Delta\delta_H$ of -NCH_2C*H*$_2CH_2$N- (ppm)	$\Delta\delta_H$ of ROAr-*t*-C_4*H*$_9$ (ppm)	$\Delta\delta_H$ of CH_3OAr-*t*-C_4*H*$_9$ (ppm)
0	0.00	0.00	0.00	*b*	*b*
5	0.01	-0.01	*a*	*b*	*b*
10	-0.03	-0.03	-0.06	*b*	*b*
15	-0.03	-0.04	-0.04	*b*	*b*
20	-0.08	-0.07	-0.13	0.00	0.00
25	-0.12	-0.11	-0.19	0.02	-0.02
30	-0.10	-0.13	-0.23	0.04	-0.03
40	-0.04	-0.18	*b*	0.06	-0.05
100	-0.10, -0.87	-0.21	*b*	0.10	-0.06

[a] the observed signal aggregates with H_2O
[b] the observed signal is not resolved
\+ indicates downfield shift
\- indicates upfield shift

adding 100 μL of DMSO-d_6, two broad singlets of *H*-N^+-*H* can be noted (which is indicative of mixed conformations). These results indicate that compound 7 in aprotic solvent possesses mixed conformations of the calix[4]arene framework. We yet cannot estimate the contribution of each conformation with the information obtained.

4.2.3 Low temperature NMR experiments in the mixed solvent

In order to reveal the mechanism of intermolecular H-bonding and ring movement, low temperature NMR experiments of 7 have been carried out at 0, -15, -25, -35 and –40 °C. The ^{1}H NMR spectra of 7 in the mixture of $CDCl_3$ and CD_3OD at various temperatures are shown in Figure 4.10. We found many interesting features of the NMR spectra. Firstly, the signal due to CD_3OH (*) shifted downfield upon decreasing the temperature. This agrees with the fact that decreasing temperature increases [73] the hydrogen bonding interactions between CD_3OH and CH_3OAr-*t*-C_4H_9 units.

Surprisingly, we did not observe a significant shift of the CH_3OAr-*t*-C_4H_9 and ROAr-*t*-C_4H_9 protons (Table 4.3). However, we observed changes in the shape of the signals due to CH_3OAr-*t*-C_4H_9 and ROAr-*t*-C_4H_9 and their aromatic correspondences.

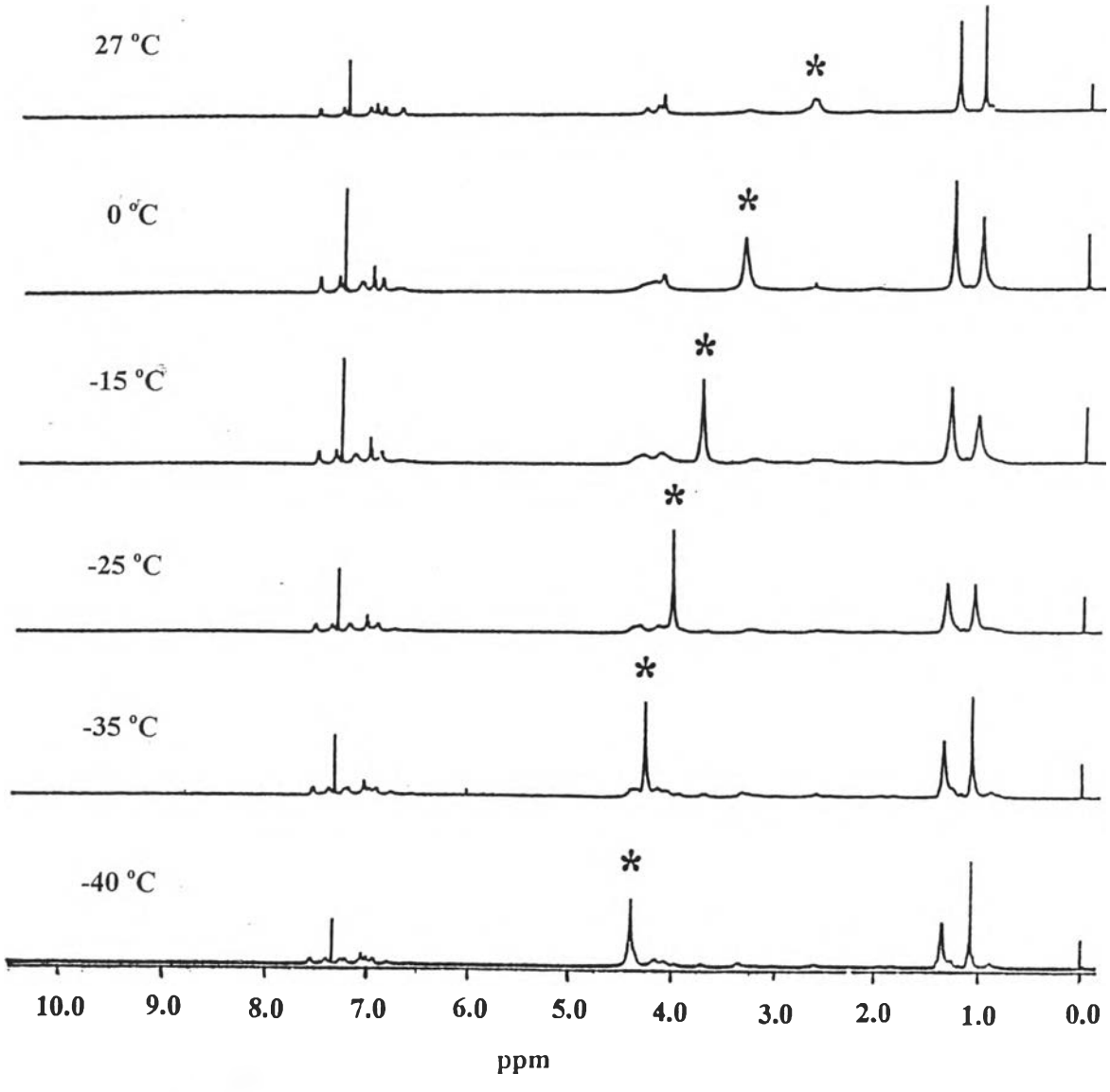

Figure 4.10 ^{1}H NMR spectra of compound 7 in the mixture of $CDCl_3$ and CD_3OD at various temperatures.

Table 4.3 Changes of the chemical shifts of $CD_3O\mathit{H}$, ROArH, $CH_3OAr\mathit{H}$, ROAr-*t*-$C_4\mathit{H}_9$ and CH_3OAr-*t*-$C_4\mathit{H}_9$ of the compound 7 in the mixture of $CDCl_3$ and CD_3OD solution at various temperature.

temperature (°C)	$\Delta\delta_H$ of $CD_3O\mathit{H}$ (ppm)	$\Delta\delta_H$ of ROArH (ppm)	$\Delta\delta_H$ of $CH_3OAr\mathit{H}$ (ppm)	$\Delta\delta_H$ of ROAr-*t*-$C_4\mathit{H}_9$ (ppm)	$\Delta\delta_H$ of CH_3OAr-*t*-$C_4\mathit{H}_9$ (ppm)
27	0.00	0.00	0.00	0.00	0.00
0	0.64	0.06	0.00	0.02	-0.01
-15	0.97	0.09	-0.04	0.04	0.01
-25	1.30	0.12	-0.02	0.05	0.03
-35	1.53	0.15, 0.11 [a]	0.00	0.06	0.03
-40	1.64	0.16, 0.11 [a]	0.00	0.06[b]	0.03

[a] the observed signal can be resolved to 2 signals
[b] the observed signal starts to resolve to 2 signals.

Enlargement of ^{1}H NMR spectra of these two regions are depicted in Figures 4.11 and 4.12. In the aromatic region the signals due to $CH_3OAr\mathit{H}$ and $ROAr\mathit{H}$ became broader when lowered the temperature. The signal due to $ROAr\mathit{H}$ shifts downfield, and at –25 °C it splits into two peaks at 7.20 and 7.25 ppm. Another signal also starts to arise at 6.97 ppm. Concurrent with the aromatic changes, we observe two pairs of doublets in 3.3-4.1 ppm region. We also notice that the signals due to CH_3OAr-t-$C_4\mathit{H}_9$ and $ROAr$-t-$C_4\mathit{H}_9$ shift slightly and become broader in which the latter splits into 2 peaks at –40 °C. These changes suggest the movement of ROArH ring from a cone to a pinched cone conformation.

From NMR studies, a possible mechanism of phenyl ring rotation (Scheme 4.1) can be proposed as follows : (1) at room temperature without intra/intermolecular hydrogen bonding, the four phenyl rings must move freely and result in a sluggish movement (within the NMR time scale), (2) in the presence of intermolecular hydrogen bonding between $CD_3O\mathit{H}$ and $CH_3\mathit{O}Ar$-t-C_4H_9, the phenyl rings are held in cone conformation and moves less sluggishly (faster than NMR time scale to detect conformational differences) and (3) at –40 °C in which the compound in the solution behaves as if it were in the solid state, the phenyl rings move very slowly (or stop) and in order to reduce the steric congestion in the calix[4]arene unit, one of the ROAr-t-C_4H_9 rings must orientate in a pinched cone conformation as shown in Scheme 4.1 (c).

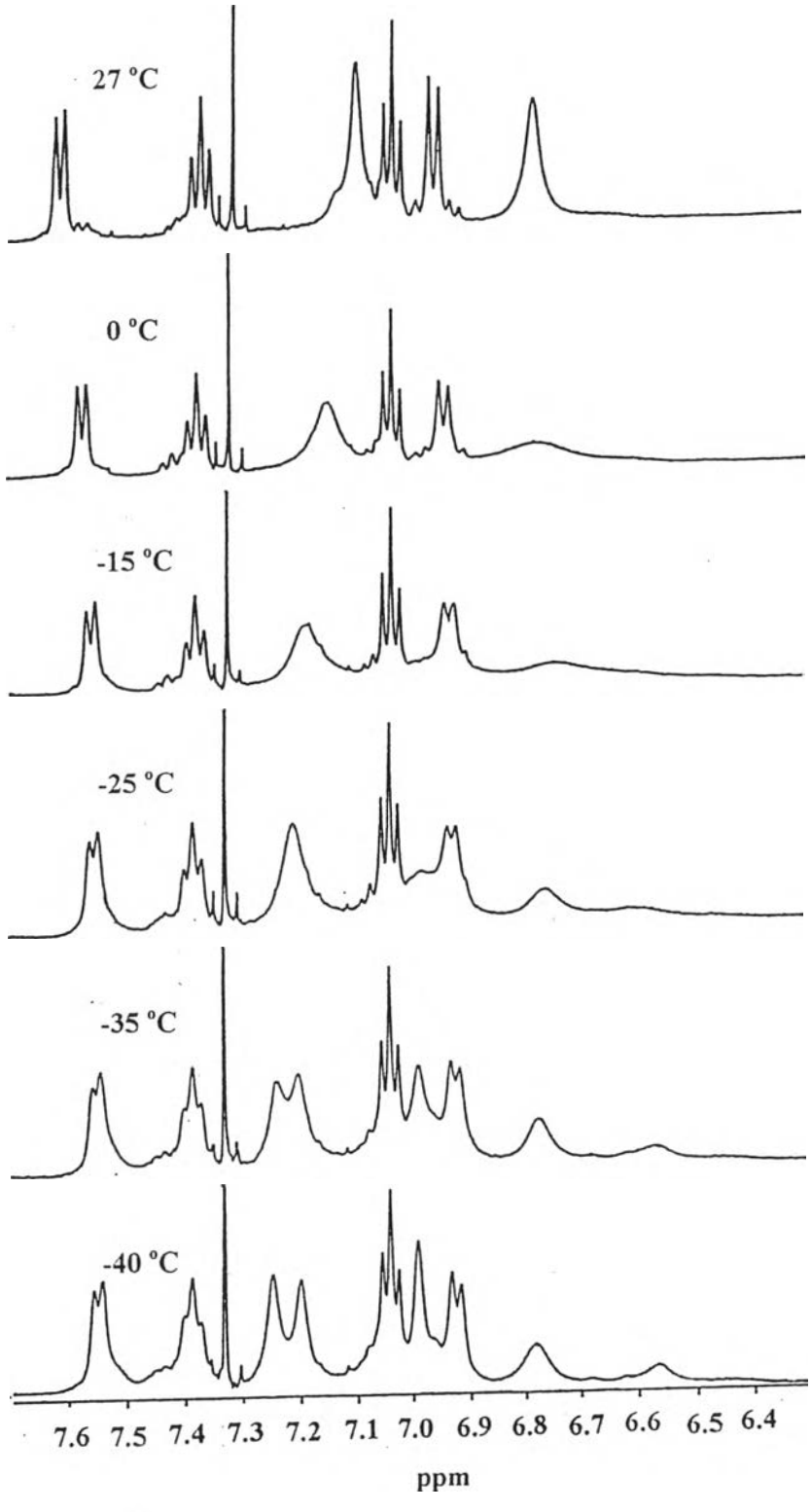

Figure 4.11 Enlargement of aromatic signals at various temperatures.

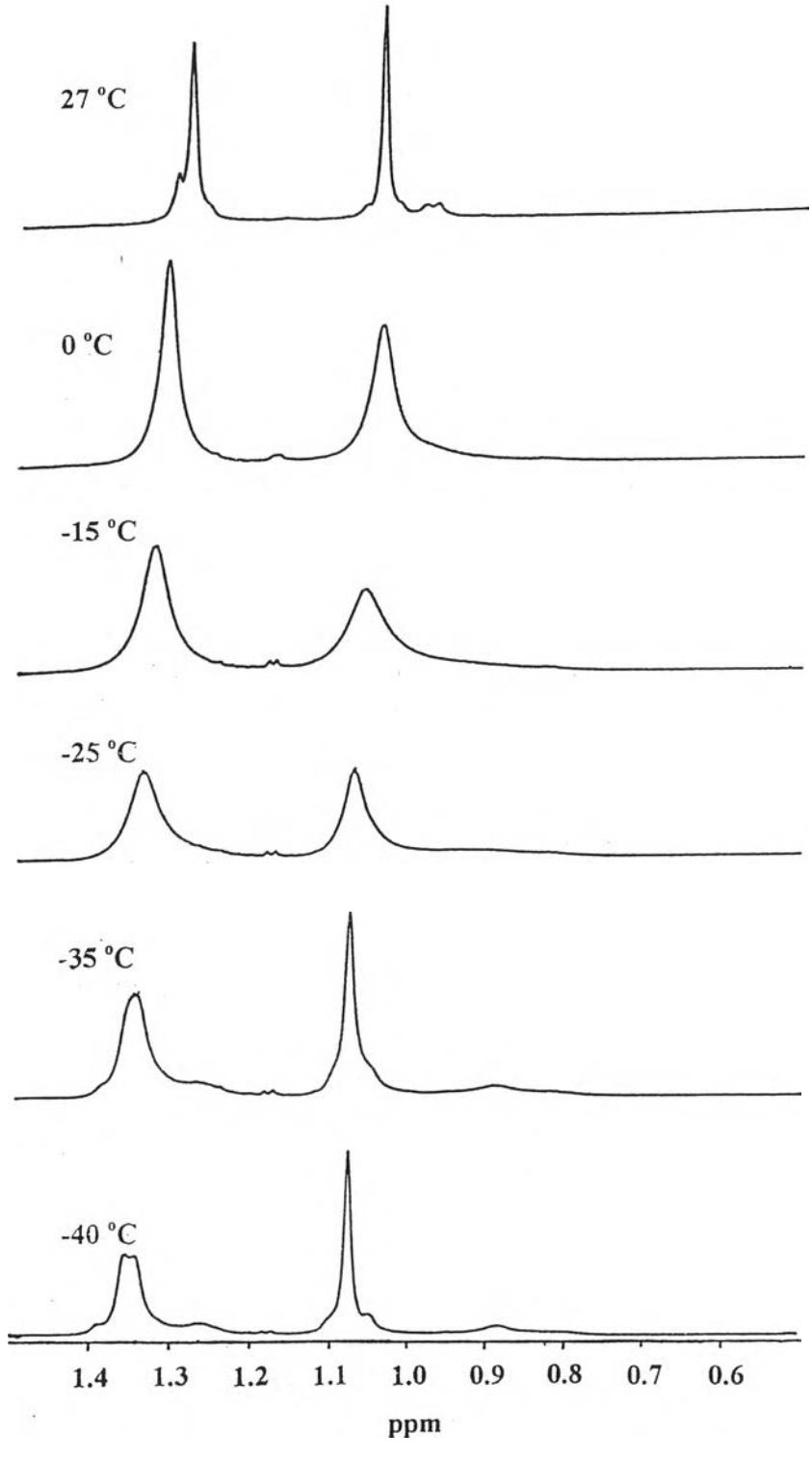

Figure 4.12 Enlargement of CH_3OAr-*t*-C_4H_9 and $ROAr$-*t*-C_4H_9 signals at various temperatures.

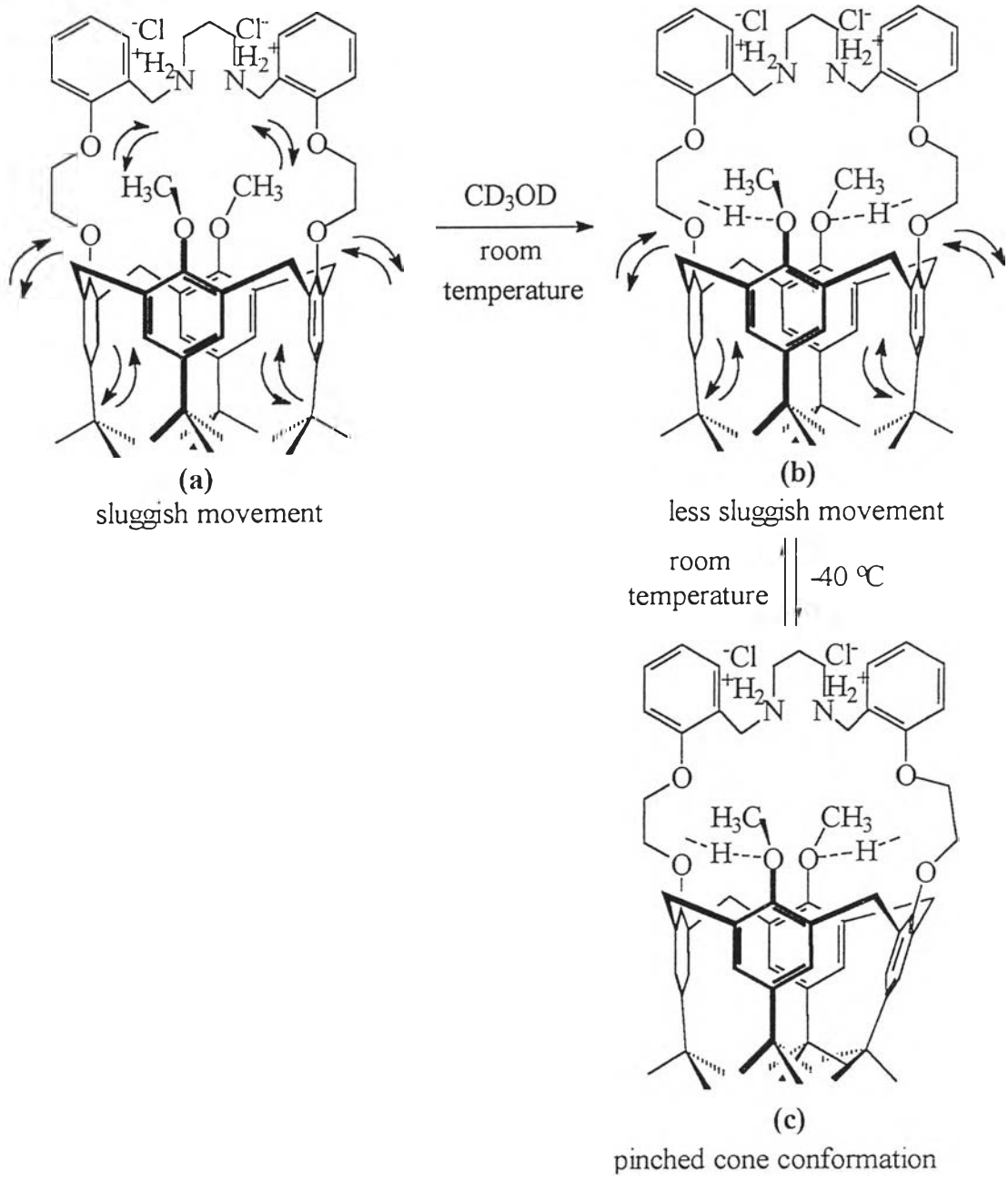

Scheme 4.1 Possible phenyl ring movement mechanism.

4.3 Basicity of 25,27-[*N,N'*-di-((2-ethoxy)benzyl)propylenediamine] -26,28-dimethoxy-*p-tert*-butylcalix[4]arene (L)

In order to study the complexation ability of 25,27-[*N,N'*-di-((2-ethoxy)benzyl) propylenediamine]-26,28-dimethoxy-*p-tert*-butylcalix[4]arene (**L**) toward Cu^{2+} and Zn^{2+}, basicity or protonation constants of the ligand **L** must be known. Protonation equilibria of **L** in CH_3OH can be defined as equations 4.2 and 4.3

$$K_1 \quad : \quad L + H^+ \rightleftharpoons LH^+ \qquad (4.2)$$

$$K_2 \quad : \quad LH^+ + H^+ \rightleftharpoons LH_2^{2+} \qquad (4.3)$$

where K_1 and K_2 are the first and second protonation constants, respectively.

In this study, potentiometric titration method was employed to calculate protonation constants of **L**. Besides the basicity of the ligand, potentiometric titration can be used to calculate some thermodynamic parameters such as ΔH or ΔS. Potentiometric titrations of **L** were carried out in methanol using Bu_4NOH as titrant base and $Bu_4NCF_3SO_3$ as inert background electrolyte. The titrations were done at various temperatures (20, 23, 25, 27, and 30 °C). Logarithm of the protonation constants of **L** at 20, 23, 25, 27, and 30 °C in methanolic solution of $1x10^{-2}$ M $Bu_4NCF_3SO_3$, evaluated by Superquad program, are shown in Table 4.4.

Table 4.4 Logarithm of the protonation constants of **L** in CH_3OH using $1x10^{-2}$ M $Bu_4NCF_3SO_3$ as inert background electrolyte at various temperatures.

Temperature		Log K_1	log K_2
°C	K		
20	293.15	10.06 ± 0.06	6.67 ± 0.06
23	296.15	9.97 ± 0.05	6.75 ± 0.12
25	298.15	9.61 ± 0.04	6.64 ± 0.11
27	300.15	9.75 ± 0.04	6.77 ± 0.10
30	303.15	9.69 ± 0.04	6.68 ± 0.10

Figure 4.13 shows titration curves of **L** at 20 °C where the ratio of concentration of **L** and proton are varied. Other titration curves of **L** at 23, 25, 27 and 30 °C are depicted in appendice (Figures A.17 – A.20), respectively. From the data obtained, $\bar{p}$ at any log $[H^+]$ can be caluculated, and their relationship can be plotted as a curve. The plot of $\bar{p}$ versus log $[H^+]$ for **L** at 20 °C is shown in Figure 4.14 (other temperatures $\bar{p}$ plots are deposited in appendice, Figures A.21 – A.24). One can observe that the shape of the plot looks like a two-step (shoulder) ladder. The first shoulder occurs approximately at $\bar{p} = 1$ and the second shoulder occurs at $\bar{p} = 2$. This indicates that **L** can be protonated in two steps (which means two log K values) to obtain the mono- and diprotonated species, respectively.

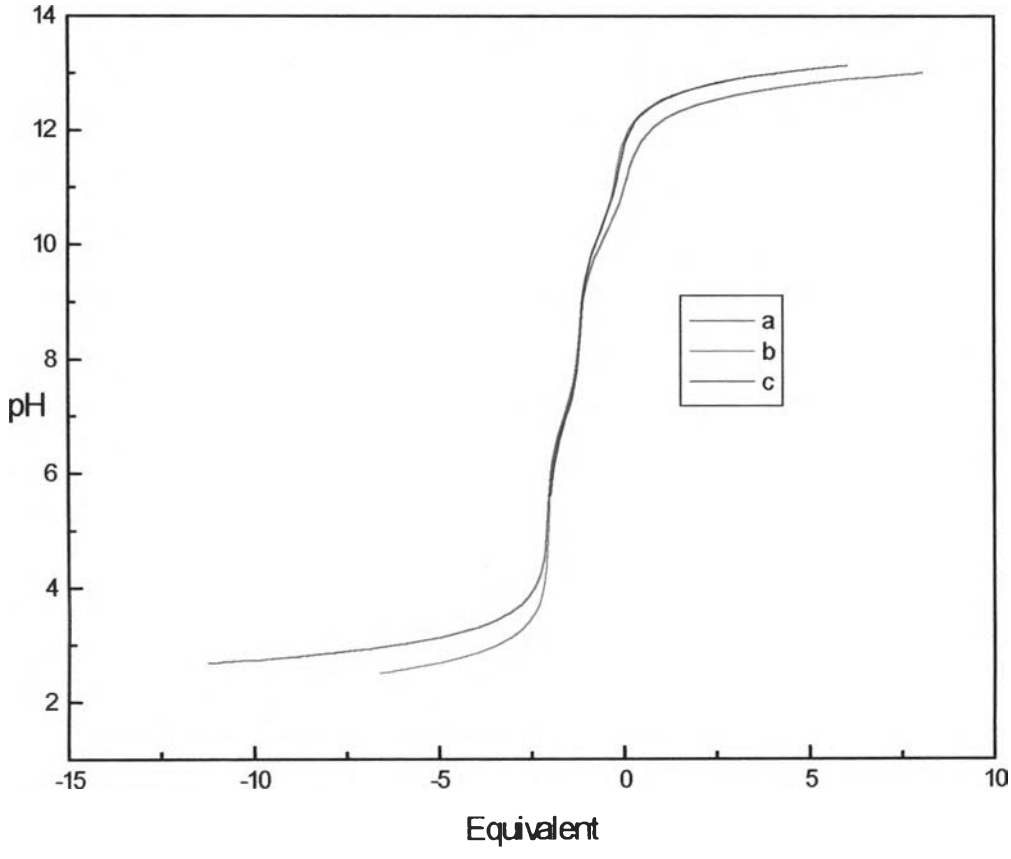

Figure 4.13 Potentiometric titration curves of **L** in the methanolic solution of $1x10^{-2}$M $Bu_4NCF_3SO_3$ at 20 °C, based on the initial concentration ratio of **L** : proton as follows : a) 0.500 mM : 5.682 mM, b) 0.914 mM : 6.084 mM and c) 0.603 mM :1.206 mM. Equivalent is defined as the ratio of $(n_{OH^-}-n_{acid})$ to n_{ligand}.

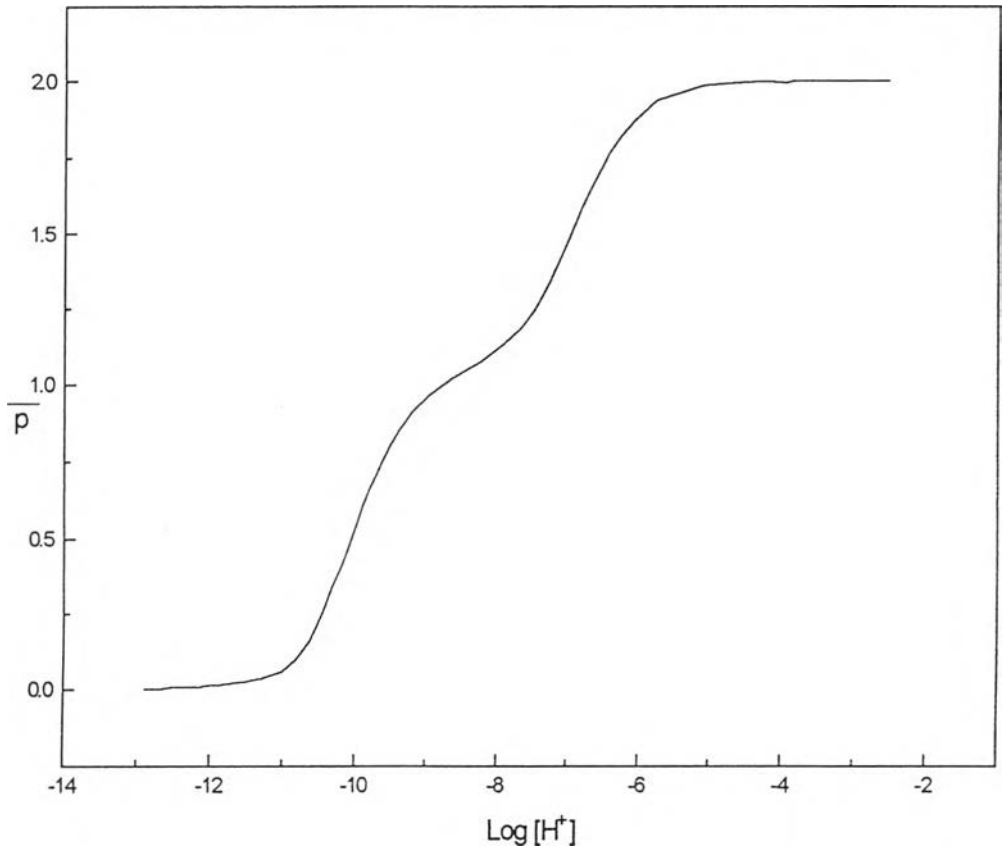

Figure 4.14 Plot between $\bar{p}$ and log [H^+] for **L** in the methanolic solution of $1x10^{-2}$ M $Bu_4NCF_3SO_3$ at 20 °C, based on the initial concentration ratio of the ligand **L** to proton of 0.914 mM : 6.084 mM.

The behaviors of each protonated species, LH^- and LH_2^{2-} can be understood by considering the species distribution curves. The species distribution curve of **L** at 20 °C in Figure 4.15 (others are shown in appendice, Figures A.25 – A.28) shows relationship of the amount of each species versus pH. The species domination is varied as LH_2^{2+} < LH^+ < **L** upon increasing pH. Other species distribution curves of **L** at other temperatures show the same trend.

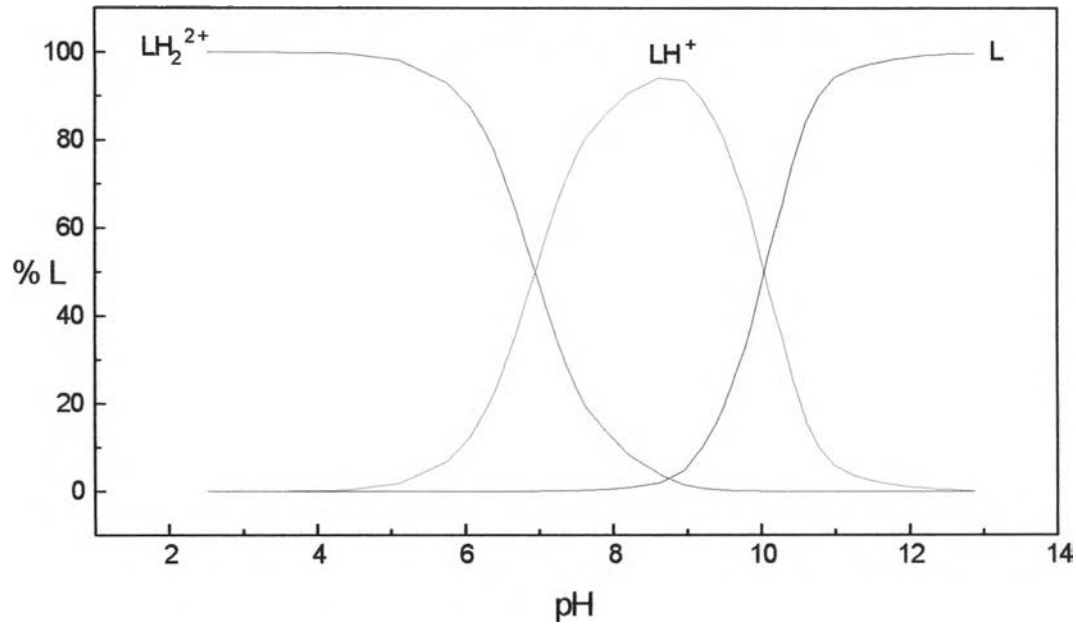

Figure 4.15 Species distribution curves of **L** in the methanolic solution of $1x10^{-2}$ M $Bu_4NCF_3SO_3$ at 20 °C, C_L = 0.914 mM.

4.4 Thermodynamic aspects of potentiometric titration data

The values of log K_1 and log K_2 for **L** at various temperatures are quite comparable. From the following basic thermodynamic equations

$$\Delta G = -RT \ln K \tag{4.4}$$

$$\Delta G = \Delta H - T\Delta S \tag{4.5}$$

Equations (4.4) and (4.5) can be rewritten as equations (4.6) and (4.7).

$$-RT \ln K = \Delta H - T\Delta S \tag{4.6}$$

$$\log K = \frac{-\Delta H}{2.303\,RT} + \frac{\Delta S}{2.303\,R} \tag{4.7}$$

The plot between log K and $\frac{1}{T}$ should give a slope of $\frac{-\Delta H}{2.303\,R}$ and intercept distance of log K at $\frac{\Delta S}{2.303\,R}$. Then, the enthalpy change, ΔH and the entropy change, ΔS can be calculated.

The plot between log K and the reciprocal of the experimental temperatures in absolute unit is shown in Figure 4.16.

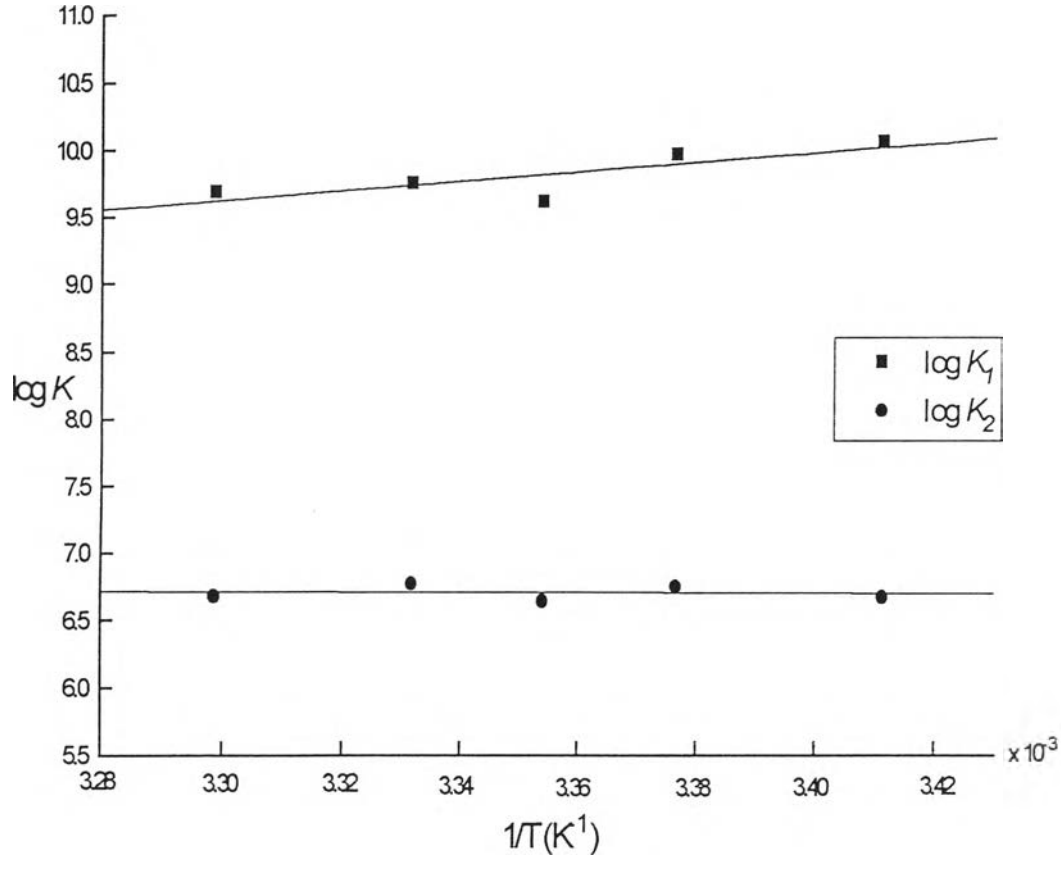

Figure 4.16 The plot between the log K of the **L** and the reciprocal of the experimental absolute temperatures.

The slope of plot of Figure 4.16 for the first and second protonations are 3,525 and –142, respectively. Their corresponding intercepts for the first and second protonations are –2.01 and 7.18, respectively . The enthalpy energy changes of the first and second protonations, ΔH_1 and ΔH_2, obtained from the slope are -67 kJ/mol and 3 kJ/mol, respectively. The entropy changes for the first and second protontions, ΔS_1 and ΔS_2, calculated from the intercepts are -38 kJ/mol·K and 137 kJ/mol·K, respectively.

The above thermodynamic values indicate that the first and second protonations are exothermic and endothermic reactions, respectively, and they occur

spontaneously ($\Delta G<0$). The total entropy changes of the first and second protonations should be positive for spontaneous reactions. The entropy change of the methanol contributing over the first protonation process should therefore be >38 kJ/mol K. These results can be concluded that the first protonation process of **L** in the methanolic solution has been strongly affected by methanol molecules. The less effect of solvation during the second protonation process is expected.

4.5 Complexation of 25,27-[*N*,*N*′-di-((2-ethoxy)benzyl)propylene-diamine]-26,28-dimethoxy-*p*-*tert*-butylcalix[4]arene (L) with Zn^{2+} and Cu^{2+} cations

The ligand **L** was then determined the complexation ability towards Cu^{2+} and Zn^{2+} ion in CH_3OH using $5x10^{-2}$ M Bu_4NOH as titrant base and $1x10^{-2}$ M $Bu_4NCF_3SO_3$ as inert background electrolyte at 25 °C. The titration curves of different initial concentration ratio of **L** to Cu^{2+} and Zn^{2+} at 25 °C are shown in Figures 4.17 and 4.18, respectively. From Figure 4.17, it shows that at the same equivalent, the titration curves of **L**:Cu^{2+} = 1:1 and **L**:Cu^{2+} = 2:1 (curves b and c, respectively) are located at lower pH than that of **L** which contains no Cu^{2+} in the solution. However, when the titration data obtained from the measurements were submitted to the SUPERQUAD program, complexes of **L** and Cu^{2+} were not found. For Zn^{2+} (Figure 4.18), the titration curves of **L**:Zn^{2+} = 2:1, c, is similar to the titration curve of ligand without Zn^{2+}, a. However, the curve of **L**:Zn^{2+} = 1:1, b, is different from the curve a. This indicates that there must be at least a Zn^{2+} complex occurred. From the process of evaluating and optimizing by SUPERQUAD program, there is only $LZn(OH)_2$ species which gives very small stability constant (log K ≈ -16). Considering the preferred coordination geometries of Zn^{2+} and Cu^{2+} which are tetrahedron and square planar, respectively, intermolecular hydrogen bonding and ring movement may prevent the ligand 7 to rearrange the donor set to tetrahedron and square planar. Therefore, the complexation between 7 and Zn^{2+} and Cu^{2+} could not occur.

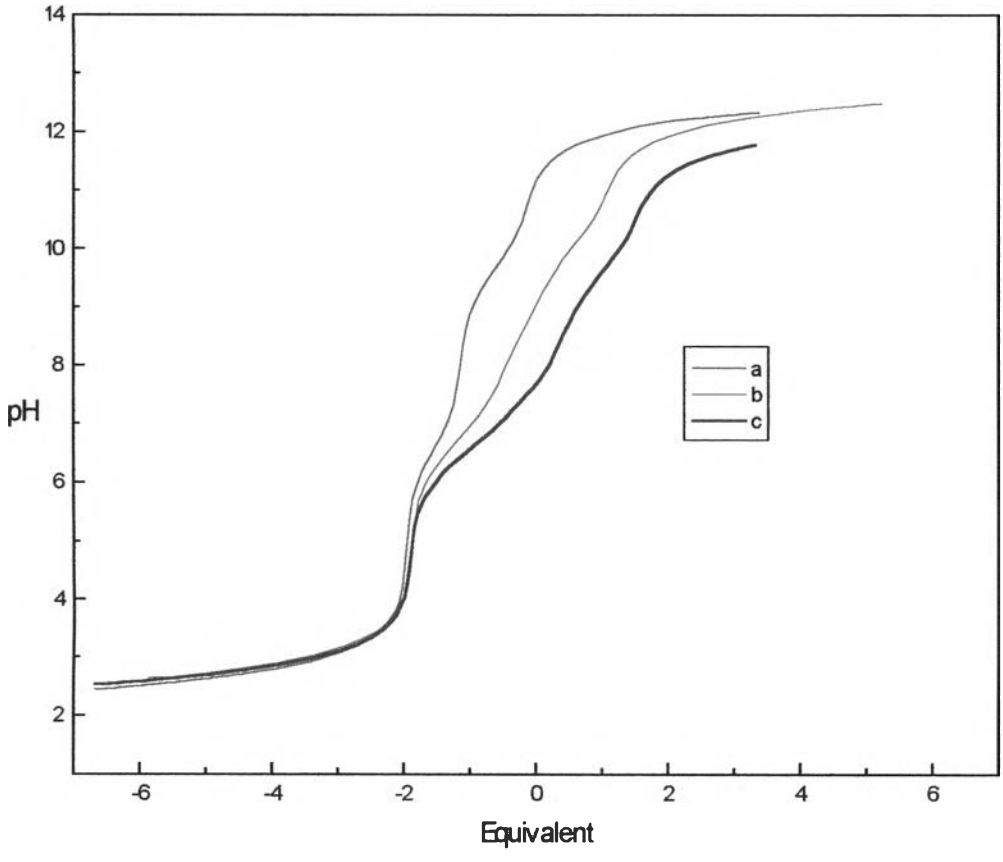

Figure 4.17 Potentiometric titration curves of **L** with Cu^{2+} in the methanolic solution of $1x10^{-2}M$ $Bu_4NCF_3SO_3$ a) at C_L = 0.909 mM and based on the initial concentration ratio of the ligand **L** to Cu^{2+} of b) 0.788 mM : 0.396 mM. and c) 0.776 mM : 0.780 mM at 25 °C. Equivalent is defined as the ratio of $(n_{OH^-}-n_{acid})$ to n_{ligand}.

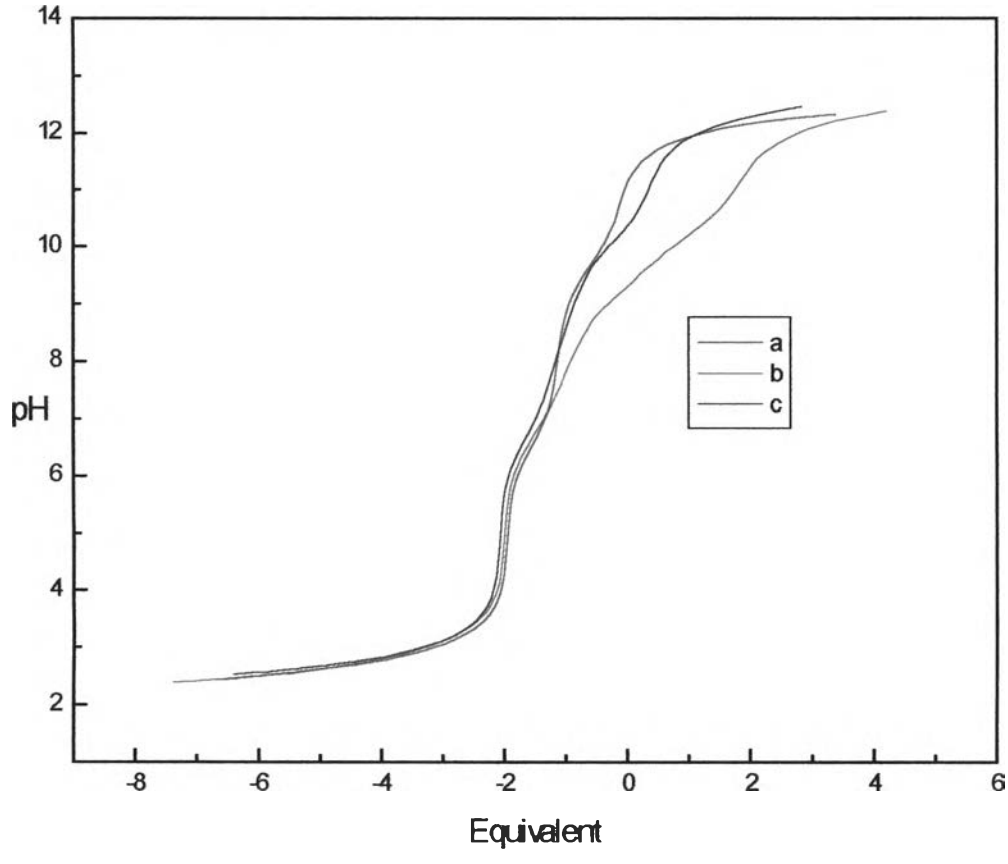

Figure 4.18 Potentiometric titration curves of **L** with Zn^{2+} in the methanolic solution of $1x10^{-2}$M $Bu_4NCF_3SO_3$ a) at C_L = 0.909 mM and based on the initial concentration ratio of the ligand **L** to Zn^{2+} of b) 0.833 mM : 0860 mM and c) 0.874 mM : 0.449 mM at 25 °C. Equivalent is defined as the ratio of $(n_{OH^-}-n_{acid})$ to n_{ligand}.